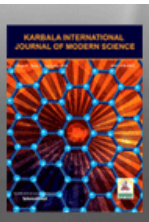

Karbala International Journal of Modern Science

Volume 10 | Issue 2 Article 2

SURFACE TREATMENTS' EFFECTS ON THE CAPACITOR'S DIELECTRIC PERFORMANCE UNDER ELECTRO-THERMAL STRESSES

Haider. M. Umran
Electrical and Electronic Engineering Department, Faculty of Engineering, University of Kerbala, Karbala, Iraq, haider.umran@uokerbala.edu.iq

Feipeng Wang
State Key Laboratory of Power Transmission Equipment and System Security and New Technology, Chongqing University, Chongqing, China

SURFACE TREATMENTS' EFFECTS ON THE CAPACITOR'S DIELECTRIC PERFORMANCE UNDER ELECTRO-THERMAL STRESSES

Abstract

Biaxial-oriented polypropylene (BOPP) films are characterized by unfavorable aging behavior because of their poor susceptibility to high temperatures, humidity, and high electric fields. This makes them unqualified to withstand harsh operating conditions, such as in capacitor applications. This study investigates the impact of annealing BOPP samples at 100 °C for five hours after fluorination at different times (15, 30, and 60 minutes) on their electrical and mechanical performance under electro-thermal stresses. Scanning electron microscope (SEM) images confirm that there is an increase in surface roughness and the formation of a dense layer of fluorine-containing groups monotonically with fluorination time. So, these roughness increases can probably change the electrical properties of the film. Based on the isothermal surface potential decay (ISPD) technique, the treated samples show slower surface potential decay than the original sample. Compared to 54% for the original sample, the surface potential remains at approximately 87.6% of its initial value after 7200 s. During aging, Fourier transform infrared (FTIR) spectroscopy and X-ray diffraction (XRD) analysis revealed changes in the surface chemical composition and crystallinity development, respectively. The treated samples show improved aging behavior in terms of a lower dissipation factor and AC conductivity compared to the original sample. In the dynamic mechanical analysis (DMA), it was demonstrated that the strong polar bonding of C-F integrated into the polymer chain enhanced film mechanical performance.

Keywords

Aging, Conductivity, Capacitor, Dielectric loss, Electro-thermal stresses, Mechanical performance

RESEARCH PAPER

Surface Modifications Effects on the Capacitor's Dielectric Performance Under Electro-thermal Stresses

Haider M. Umran [a,b,*], Feipeng Wang [b]

[a] Electrical and Electronic Engineering Department, Faculty of Engineering, University of Kerbala, Karbala, Iraq
[b] State Key Laboratory of Power Transmission Equipment and System Security and New Technology, Chongqing University, Chongqing, China

Abstract

Biaxial-oriented polypropylene (BOPP) films are characterized by unfavorable aging behavior due to their poor susceptibility to high temperatures, humidity, and electric fields. This makes them unqualified to withstand harsh operating conditions, such as in capacitor applications. This study suggests chemical and physical surface treatments to enhance the BOPP film's resistance to aging. The treatments include annealing the samples at 100 °C for five hours after being fluorinated at different times (15, 30, and 60 min) and then investigating their electrical and mechanical performance under electro-thermal stresses. The increase in surface roughness and the formation of a monotonically dense layer of fluorine-containing groups during fluorination are revealed by scanning electron microscopy (SEM). These roughness increases can probably change the electrical properties of the film. Based on the isothermal surface potential decay (ISPD) technique, the treated samples show slower surface potential decay than the original sample. Compared to 54% for the original sample, the surface potential remains at approximately 87.6% of its initial value after 7200 s. Fourier transform infrared (FTIR) and X-ray diffraction (XRD) analyses reveal changes in the surface chemical composition and crystal development. The decreased dissipation factor and AC conductivity of treated samples exhibit improved aging behavior. The strong polar bonding impact of the CF bonds incorporated with the film chain on enhancing its mechanical performance is confirmed by dynamic mechanical analysis (DMA).

Keywords: Aging, Conductivity, Capacitor, Dielectric loss, Electro-thermal stresses, Mechanical performance

1. Introduction

Because of their distinct electrical properties and chemical and thermal stability, biaxial-oriented polypropylene (BOPP) films have been considerably used in capacitor technology. They possess a low dielectric loss (tan δ), typically 2×10^{-4} for 0–85 °C, and a high breakdown strength of up to 730 V/μm or an electric field strength of 81 V/μm [1]. These dielectric polymers are therefore among the most critical parts of the structure of the metalized polypropylene (MPP) capacitor. MPP capacitors are typically made of two PP films coated in a nanometer-thick metal layer of aluminum or zinc-aluminum alloy wrapped around a hollow mandrel [2]. On each edge, there is one thin area that is non-metalized (i.e., the margin). In contrast, on each end of the winding is a sprayed-on metal schoopage [3]. This allows each film to connect with only one side and isolate the two films from each other. The cylindrical-type MPP capacitor construction is depicted in Fig. 1.

These films are semi-crystalline thermoplastic polymers with the chemical formula (C_3H_6) n and have chemical structures shown in Fig. 2. They therefore consist of a linear hydrocarbon chain and an alternating methyl group [4].

Received 24 November 2023; revised 19 March 2024; accepted 29 March 2024.
Available online 25 April 2024

* Corresponding author at: Electrical and Electronic Engineering Department, Faculty of Engineering, University of Kerbala, Karbala, Iraq.
E-mail address: haider.umran@uokerbala.edu.iq (H.M. Umran).

https://doi.org/10.33640/2405-609X.3348

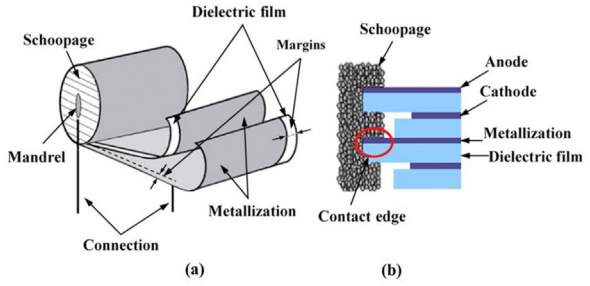

Fig. 1. Construction of a cylindrical MPP capacitor: (a) structural components and (b) contact edges cross-section (replotted from Ref. [3]).

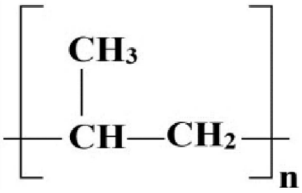

Fig. 2. Chemical structure of Polypropylene (replotted from Ref. [4]).

The microscopic structure and dynamic properties of the polymer primarily determine its electrical and mechanical performance during application [5,6]. Irregular molecular arrangements of oriented polymers cause the microstructural defects that create weak points within the film, ultimately leading to their failure. These defects help create space charge traps, which have cascading impacts on the dielectric, such as local electric field distortion and electromechanical stresses, and thus aging [7]. Even though metallized BOPP has a unique capacity for self-healing, a high temperature and electrical fields cause partial frequent discharge, resulting in flashover events and ultimately irreversible breakdown [1,8].

This type of polymer film has a tertiary proton in each monomer unit, making it more vulnerable to degradation by free radicals. When the polymeric radical C is exposed to prolonged high temperatures and/or high electric fields, it spontaneously oxidizes to produce peroxy radicals (ROO). This process also involves the removal of the hydroperoxide group (-OOH) and tertiary hydrogen (H*). Two pairs of low-molecular-weight PP chains are produced, and subsequent decomposition of the (-OOH) is caused by two possible mechanisms of polymer chain degradation [9]. The formation mechanism of ROO and −OOH groups after the removal of H* and the oxidation of O for the C radical is illustrated in Fig. 3.

As a result, BOPP films have been classified as dielectric polymers with unfavorable aging behavior in applications involving harsh environments [1]. In

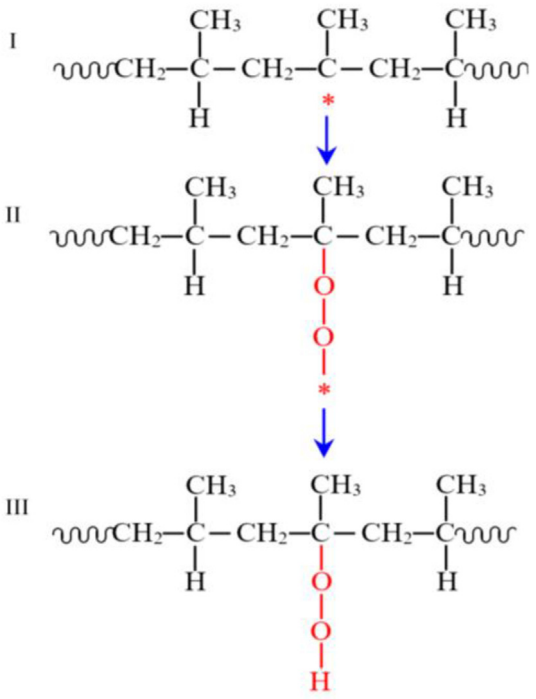

Fig. 3. Formation mechanism of ROO and −OOH groups after H removal and O oxidation of the C radical (replotted from Ref. [9]).*

this regard, enhancing the aging behavior of BOPP films has not received significant attention in the literature. Many works have attempted to improve the various properties of polymers depending on their applications using techniques of micro- and Nano-fillers. For several factors, including the difficulties of uniformly dispersing fillers, the stress concentration within the polymer matrix, advanced and expensive incorporation techniques, and achieving balancing between their contradictory properties. In addition to the problems related to fillers' compatibility with the polymer matrix and the polymer's dimensional stability under different environmental conditions, these techniques were classified as difficult and complex. Thus, the above factors all significantly impact the polymer's ultimate electrical, mechanical, and physical properties [10–12].

Compared to others, gas fluorination is one of the easiest and most effective techniques to modify the molecular structure of the polymer surface layer and may enhance its mechanical and electrical characteristics. According to related results, fluorination can improve the charge transfer characteristics of polymeric films by altering the molecule structure. This lowers the interfacial electric field and actively suppresses space charge injection and accumulation within the film [13,14]. Also, fluorination can increase the depth and density of the surface traps,

significantly reducing the electric field close to the electrode by a sizable amount of the homocharges trapped in the traps [15]. When fluorine atoms are introduced into the structure of a polymer film, they reduce its surface energy due to their high electronegativity, producing a surface that repels water. Reducing the film's moisture absorption by enhancing its hydrophobicity preserves its electrical properties. Enhancing the polymer's moisture resistance that is used in insulation makes it less likely to degrade over time and ensures consistent performance [16,17].

In contrast, annealing BOPP films would alter their crystal structure and increase crystallinity, which could ultimately enhance their mechanical and electrical properties [18]. This process can enhance the tensile strength and elongation at the break of films and relieve internal stresses, improving their mechanical stability. Annealing also improves the film's heat resistance, which increases its thermal stability and enhances its performance, particularly at higher temperatures [18,19]. Improved crystalline–amorphous interface regions and/or increased crystallinity are two more benefits of annealing [20]. Therefore, annealing can enhance the structural properties of semi-crystalline polymers and, consequently, improve their electrical properties [21].

The main objective of this study is to enhance the electrical and mechanical performance of BOPP film under electro-thermal stresses by altering its chemical composition and crystal structure. The enhancement of the film's performance is to increase its ability to withstand temperatures and electric field strengths for the long haul above conventional values (i.e., above 85 °C and 81 V/μm) without substantially increasing dielectric loss [22]. One of the most significant challenges facing BOPP mechanical performance under applied stresses on the capacitor is maintaining its elasticity or resistance to mechanical deformation. Accordingly, this study proposes film surface treatments that include fluorination and subsequent annealing. The impact of the introduction and interaction of the C–F group on the film surface and its effect on producing charge traps and suppressing charge decay were discussed. Also, the morphological, chemical, and crystalline changes and surface charge behaviors before and after treatments were studied. The mechanical and electrical properties of the film under electro-thermal stresses were studied using dielectric relaxation spectroscopy (DRS), AC conductivity, and dynamic mechanical analysis (DMA).

2. Experiment procedures

2.1. Materials and sample preparation

Due to the capacitance being inversely proportional to the distance of the capacitor plates, a thinner dielectric provides higher capacitance in a smaller volume. The performance of capacitors is significantly dependent on the film thickness, which in turn affects dielectric absorption, high-frequency susceptibility, charge and discharge times, energy losses, and structural defects. Yet, efficiency and energy density increase as a result of their ease of winding more tightly. On the other hand, thinner films age more quickly under higher voltage stress [22]. Accordingly, a semi-crystalline BOPP film with a thickness of 9 μm was selected in this study. The film samples were subjected to surface chemical and thermal treatments to enhance their mechanical and electrical properties. Samples were washed with full-concentration ethanol before treatment and then dried overnight at 30 °C. Using an inert gas and a fixed combination of 5% F_2 + 95% N_2, fluorination was carried out inside a sealed stainless steel vessel at 25 °C for exposure times of 15, 30, and 60 min. After that, the fluorinated samples were annealed at 100 °C for 5 h.

Samples were subjected to DC electro-thermal stresses for 500 h in two cycles on a test platform specifically designed for this purpose in order to evaluate the effectiveness of the treatments applied. The first cycle is 250 h with 80 V/μm at 85 °C, while the second one is 250 h with 100 V/μm at 100 °C. To abbreviate in the later texts, the aged pure sample was coded as PG, while the original and annealed samples after fluorination at different times (15, 30, and 60 min) were coded as Pure, FA1, FA2, and FA3, respectively. The specifications of the samples and related test preparations are listed in Table 1.

2.2. Chemical structure analysis

The film's chemical composition alterations are detected, and the polar groups are evolved using Fourier transform infrared spectroscopy (FTIR) (Broker Alpha, Germany). This analysis technique uses infrared light to scan samples and detect the chemical and bonding properties of polymeric materials. Thus, part of the infrared radiation that passes through the various molecules that compose the material structure is absorbed. This technique produces different spectra that can be used to identify and differentiate among molecules. Yet, the

Table 1. Specifications of BOPP samples and related test preparations.

	Pure	FA1	FA2	FA3	PG
Testing	Untreated sample	Fluorinate for 15 min, then anneal for five hours at 110 °C.	Fluorinate for 30 min, then anneal for five hours at 110 °C.	Fluorinate for 15 min, then anneal for five hours at 110 °C.	Aged pure sample due to electro-thermal stresses for 500 h on two equal cycles of 250 h.
SEM	Sample size: 4 × 4 mm. Coated with 13 nm-thick gold.				
ISPD	Sample size: 25 × 25 mm. Coated on one side with gold, 25 nm thick and 20 mm in diameter.				
FTIR	Sample size: 10 × 10 mm.				
XRD	Sample size: 10 × 10 mm.				
DSR	Sample size: 15 × 15 mm. Coated on two side with gold, 20 nm thick and 10 mm in diameter.				
DMA	Sample size: 10 mm × 6 mm.				

chemical structure of BOPP could alter as a result of the applied electro-thermal stresses.

Regardless, testing was carried out with a scan range of 4000–500 cm^{-1}. Four scans per sample were applied with a resolution of 4 cm-1 (i.e., spectra obtained at intervals of about 2 cm^{-1}) without prior special preparation.

2.3. Morphological, crystalline, electrical, and mechanical measurements

A scanning electron microscope (SEM, JEOL JSM-7800F) was used to analyze the surface morphology changes both before and after surface treatments. In contrast, variations in the crystal structures during the application of stresses were identified by X-ray diffraction on a Rigaku DMAX/2500 diffractometer (Rigaku, Woodlands, TX, USA) using an X-ray source with an incident wavelength of 1.5406 Å. Using the peaks and baseline analysis approach offered by the Origin Lab software, crystalline peaks were determined as a first step. The crystalline peaks' areas were summed using Excel to calculate the total crystalline phase. Using the Origin Lab software again, the total areas of the crystalline and amorphous phases were computed for each peak in the second stage. Finally, the crystallinity percentage was calculated for each sample using Excel again. On the other hand, utilizing dielectric relaxation spectroscopy (DRS, Novocontrol GmbH, Germany), dielectric performance was confirmed. The dielectric losses (tan δ) of Pure and treated samples were measured as a function of frequency during electro-thermal stressors. The measurements were performed in the frequency range of 0.01–10 MHz at a room temperature of 25 °C and a relative humidity (RH) of about 30%. Meanwhile, the temperature dependence of mechanical properties was measured using DMA (Q800 DMA, TA Instruments). The DMA technique has been widely used to calculate the kinetic properties of a material by measuring the strain or stress that is produced from the strain or stress oscillating over time due to cyclically applying small deformations. This makes it possible to examine the material's response to stress, temperature, frequency, and other parameters. Therefore, the value of this test lies in its ability to simulate the material's working conditions, allowing forecasting of its behavior under the application. In this regard, the measurements were made at temperatures ranging from −40 °C to 160 °C with a heating rate of 2 °C per minute at 1 Hz.

2.4. Potential decay measurement

The isothermal surface potential decay (ISPD) technique was extensively used to study surface charge dynamics and charge trapping characteristics within dielectrics. Charges accumulate on the dielectric surface during this process, and when low-energy electrons briefly polarize it, surface potential develops. The charges on the surface are accelerated to flow into the material after depolarization. This permits an analysis of the behavior of dynamic surface potential and the measurement of fast and slow potential charge decay [23]. The surface potential decay measurement equipment employed, however, is depicted in Fig. 4.

To ensure close contact during charging and measurement, samples were coated on one side

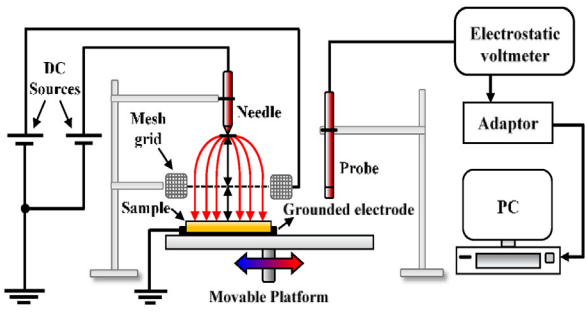

Fig. 4. Experimental setup for surface potential decay measurement.

with a thin layer of gold that was 20 mm in diameter. The sample was instilled on a moveable platform beneath a needle electrode that was 13 mm long and 8 mm from the mesh grid. The DC voltages of 8 kV and 4 kV were supplied to the needle electrode and mesh grid, respectively, to polarize for 10 min. A TREK model 542A electrostatic voltmeter was used to measure potential decay for three hours at 25 °C.

2.5. Electro-thermal stresses

According to the planned stress cycle, the test platform was carefully constructed to guarantee that thermal and electrical stresses are applied simultaneously. Two 45 × 45 cm perpendicular polyvinylidene fluoride heat-resistant panels served as the test platform. On the platform, four parallel electrodes were constructed to simulate a real capacitor on a lab scale. A thin gold layer with a diameter of 10 mm was vaporized on one side of each of the two opposing samples included on each electrode. Hence, the test platform was put into a precisely controlled air-circulation oven supplied with DC voltage. Still, a heat-resistant wire up to 140 °C with a diameter of 1.32 mm was used to connect the DC source to the positive electrodes, while a flexible flat copper tape of size 4 mm^2 was used as the ground.

3. Results and discussion

3.1. Surface morphology analysis

The cross-section images of treated samples are illustrated in Fig. 5. These images reveal the ability of fluorine to cause surface morphological alterations and penetrate narrow regions of the sample surface (i.e., light-colored regions).

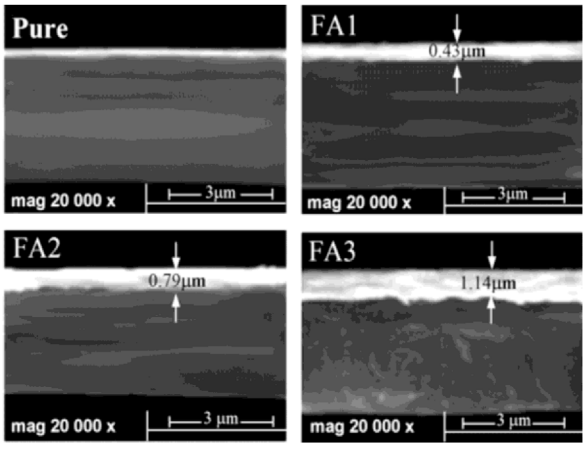

Fig. 5. SEM cross-section images of pure and treated samples.

This activity may help relieve physical defects like nanopores and cavities, which enhance dielectric performance. Fluorination produced a rougher surface than the pure sample, which is advantageous for enhancing contact with the dielectric surface. As the fluorination time advanced, the samples FA1, FA2, and FA3 demonstrated an increase in the fluorine layer by 0.43, 0.79, and 1.14 μm, respectively. As a result of C–F bond interactions on the FA3 surface sample, its surface morphology altered significantly compared to other samples. This increase can advance the possibility of water molecule adsorption and increase the surface oxygen content, ultimately degrading dielectric performance.

3.2. Surface-potential decay

The surface potential is formed when charges accumulate on the surface of the dielectric after it has been exposed to low-energy electrons for a short period of time. The surface charges will be accelerated after the irradiation to flow into the substance [21]. In this regard, the injected charges follow two different behaviors: some will get trapped in the trap centers, while others will drift through the conduction band to the opposite electrode [24,25]. These charge behaviors have a substantial impact on the dielectric's performance during application. The samples' typical normalized surface potential decay curves are shown in Fig. 6. By dividing the surface potential at every given time by the initial surface potential of the samples, the normalized potential decay was computed, which directly explains the potential decay characteristics. Regardless, after 7200 s, the surface potentials of the samples Pure, FA1, FA2, and FA3 dropped to 54%, 77.2%, 87.6%,

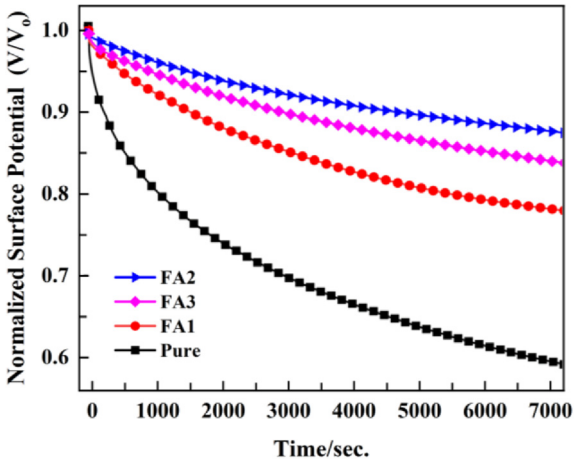

Fig. 6. Normalized surface potential decay curves of pure and treated BOPP samples before application of electro-thermal stresses.

and 82%, respectively, from their initial potentials. The surface charge density is associated with the rate of fluorine deposition on the sample surface, which decreases over time (i.e., from 0 to 30 min). This increase in the surface charge rate is attributed to the charge being easily and quickly de-trapped from the trapping sites. Fluorine has the ability to alter the surface state and shift traps from deep to shallow at the surface [26,27].

On the other hand, as the fluorination time increased to 60 min, the fluorine changed the surface chemical composition and created defects and deeper traps on the sample surface. This resulted in a lower rate of charge decay because the charge trap and release processes would take longer periods of time, unlike those in the sample fluorinated for 30 min. Further, because deeper traps are qualified to trap larger charge amounts, this will increase the likelihood of charge injection and accumulation within the film. The increased crystallinity resulting from annealing helped increase charge stability due to the difficulty of charges escaping from deep traps [20]. Consequentially, the surface charge behavior is enhanced as a result of changes in the chemical and crystal structures of the dielectric.

3.3. Chemical and crystal structure

Surface chemical structural changes resulting from electro-thermal stresses in the Pure and treated samples were investigated using FTIR spectroscopy analysis. The wavenumber range of the characteristic vibration peaks of the saturated C−H bonds was specified from 2950 to 2837 cm^{-1}. The locations of the $C-H_2$ deformation vibration peak and the $C-H_3$ symmetrical deformation peak were specified at 1454 cm^{-1} and 1375 cm^{-1}, respectively. Meanwhile, at wavelengths ranging from 3800 to 3100 cm^{-1} and from 1900 to 1600 cm^{-1}, carbonyl (C═O) and hydroxyl (-OH) groups were specified, respectively [26]. Still, the spectra of the pure, treated, and stressed samples are presented in Fig. 7.

The characteristic absorption peaks of the PG sample exhibited a noticeable intensification, indicating alterations to the molecular and compositional structure. The alterations were manifested by the formation of C═O and −OH groups, as well as an increase in crystallinity compared to the pure sample. These are a result of a combination of factors, including thermal degradation, oxidation, and the existence of decomposition products. The spectra of the treated FA1, FA2, and FA3 samples showed a non-monotonic reduction in the characteristic absorption peaks with an increased fluorination time of 15−60 min. This decline indicates that the weaker C−H bonds, with a bond energy of 414 kJ/mol, were broken as a result of the strength of the C−F bonds, with a bond energy of 544 kJ/mol [26].

The spectra of the FA1, FA2, and FA2 samples exhibited the formation of prominent broadband distinctive peaks at 1300−1020 cm^{-1}. The increased fluorine concentration on the surface causes the saturated C−H bonds to break and the formation of the C−F groups. Elemental substitution, chain cleavages, and cross-linking reactions are combined to alter the surface properties of samples. The fluorine's high electronegativity led to strong polar bonding between C and F that could contribute to improved film thermal stability. Under applied stressors, fluorine encouraged the cleavage of the long chains, which produced polar groups. In this regard, the FA1 sample's spectra revealed a marked rise in the peaks of saturated C−H bonds compared with the treated. This demonstrated the formation of new chemical bonds resulting from those stresses. These stresses broke the C−F bonds, reducing the intensity of the absorption peaks associated with these bonds and revealing the degradation of the molecular structure. Meanwhile, the FA2 spectrum showed the crystallinity and characteristic peaks of the C−H and C−F groups increasing during treatments. The FA2 sample surface's C−F bond accumulation resulted in a denser molecular conformation. This helped prevent the injection of further charge from the electrode under the stresses, thus lowering the absorption density of the polar groups. The stresses encouraged cross-linking processes and the formation of new chemical bonds, which intensified characteristic absorption peaks.

On the other hand, the AF3 sample revealed a reduction in the characteristic peaks of the C−H and a significantly increased C−F group peak. Fluorination at high deposition rates (i.e., 60 min) can break the surface chemical structure of the polymer film. This could allow oxygen to permeate the surface layer and accelerate oxidation processes as stresses are applied. Consequently, the spectra of the FA3 sample revealed a marked increase in the polar groups' intensity. Moreover, the high deposition rate contributed to increased absorption peaks of the crystalline phase at 997, 899, and 841 cm^{-1} [28]. It is found that the optimal fluorine layer (i.e., at 30 min) significantly influences slowing down the aging reactions caused by the impact of applied stresses. By producing a stable, inert surface that inhibits the formation of free radicals and the penetration of reactive oxygen species (ROS). The fluorine layer acts as a barrier, shielding the polymer from degradation and extending the film's lifespan.

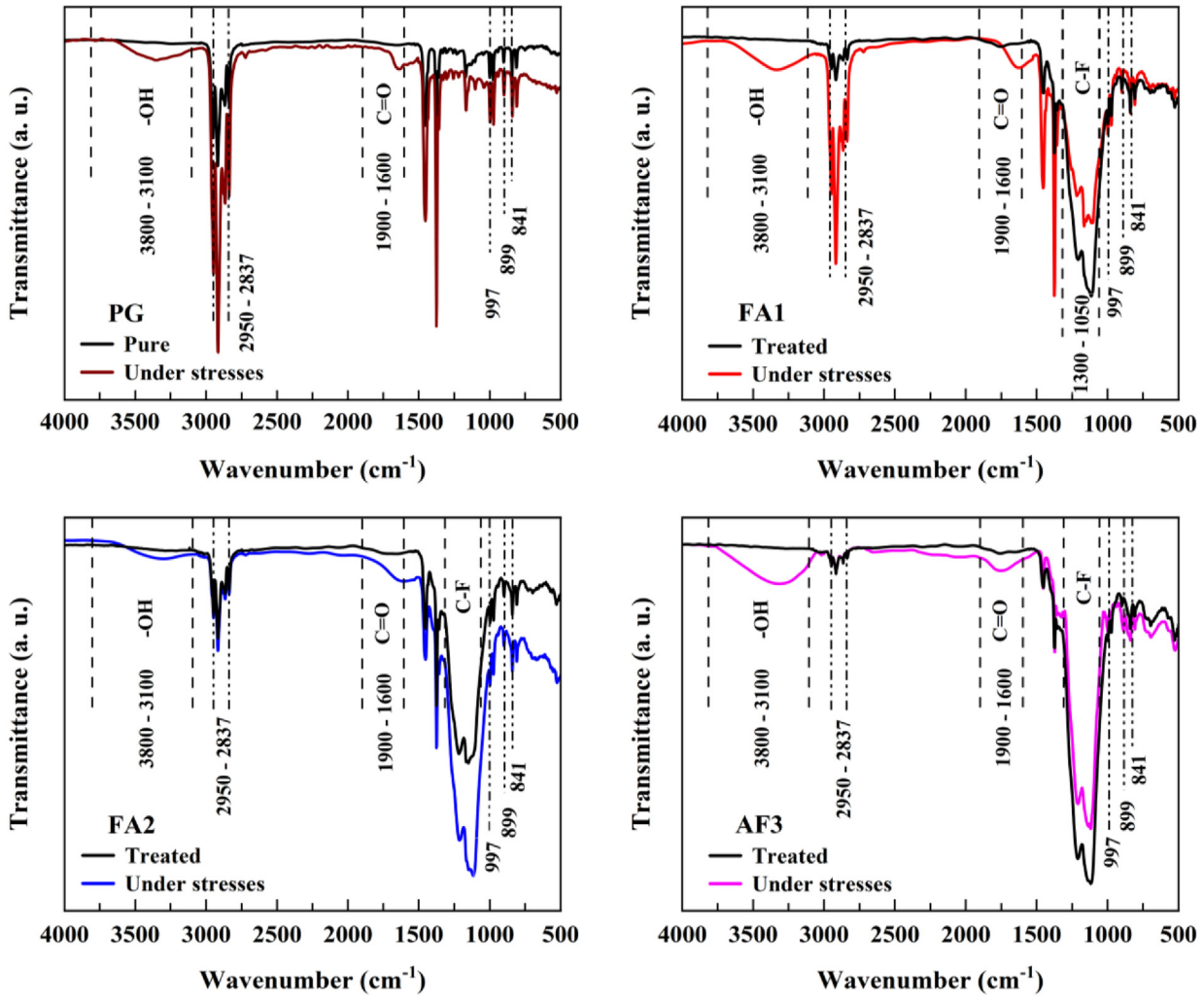

Fig. 7. FTIR spectra of Pure, treated, and electro-thermally stressed BOPP samples.

Using X-ray diffraction (XRD) analysis, the characteristics of the crystal structure of the BOPP samples were studied under electro-thermal stressors. The XRD patterns of the samples are displayed in Fig. 8. Meanwhile, the calculation results for crystallinity, reflection angle, and interplanar spacing are detailed in Table 2. The reflection angles and corresponding interplanar spacing were calculated based on Bragg's law ($n\lambda = 2d \sin\theta$). Where the X-ray source's wavelength λ, the reflection angle θ, and the interplanar spacing d in angstroms (Å) are the law's parameters. The crystallinity formula given in equation (1) was used to calculate the total crystallinity percentage for each sample.

On the XRD spectra of PP film, the characteristic reflections (110), (040), and (130) of the α-crystals

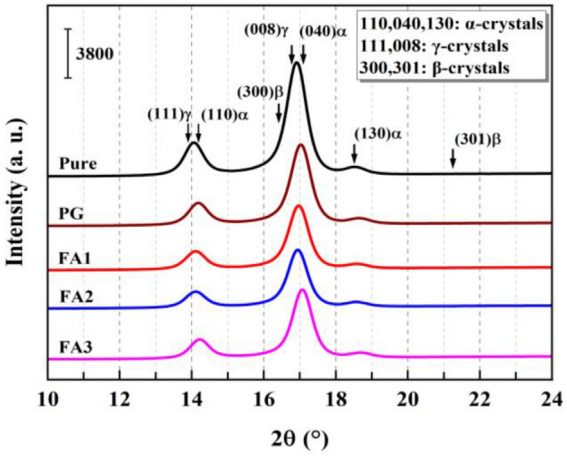

Fig. 8. XRD patterns for the Pure and treated BOPP samples during the application of electro-thermal stresses.

$$\text{Crystallinity} = \frac{\text{Area of crystalline peaks}}{\text{Area of all peaks (crystalline + amorphous)}} \times 100 \quad (1)$$

Table 2. Crystallinity, reflection angle, and interplanar spacing results for BOPP samples.

Samples	Crystallinity	2θ (°)	Interplanar spacing (Å)
Pure	68.1%	13.94, 16.80	6.348, 5.273
PG	79.3%	14.16, 17.03	6.249, 5.205
FA1	78%	14.11, 16.88	6.272, 5.248
FA2	78.2%	14.12, 16.94	6.267, 5.229
FA3	79.5%	14.15, 16.98	6.254, 5.218

typically appear as characteristic peaks at 2θ equal to 14.10°, 17.05°, and 18.61°. The γ-crystals' reflections (111) and (008) are at 13.84° and 16.71°. In contrast, the β-crystals' reflections (300) and (301) are located at 13.84° and 16.71°, respectively [29–31]. In this regard, analysis of the stressed samples revealed that the reflection peaks (110, 141, and 130) of the α-crystals decreased in both intensity and width. Compared to the 13.94° and 16.80° of the Pure sample, the two peaks of the diffraction angle increased by 0.22° and 0.23° for the PG sample.

In contrast, they increased by 0.01° and 0.06° for the FA1 sample and 0.03° and 0.04° for the FA3 sample, compared to 14.12° and 16.94° for the FA2 sample. On the other hand, the XRD pattern analysis revealed that the electro-thermal stresses have a significant impact on crystallinity and corresponding interplanar spacing. In comparison to the Pure sample, the crystallinity of the PG sample increased dramatically by 16.4%. The FA1, FA2, and FA3 samples, however, showed varying increases in crystallinity of 14.5%, 14.8%, and 16.7%. The fluorine atoms on the surface may also help pack and arrange polymer chains.

The significant crystallinity observed in PG may be due to the rearrangements of crystalline regions. These events result from chain cleavages and developments in crystal size resulting from the crystallization of the amorphous phase fraction. Given that the interplanar spacing values are falling, it implies that the chain spacing is also shrinking, and cross-linking becomes more likely. Regardless, fluorine can help encourage stronger inter-molecular interactions, which promote the hardness and strength of the samples. Interestingly, alterations in crystal structure had imposed effects beyond those of chemical composition [20].

This implies that the charge traps of the dielectric have a major influence on the trapping, de-trapping, transport, and generation of space charges. Chemical defects, such as impurities, defects in amorphous and crystalline regions, and chain termini of macromolecules, may all serve as charge traps. Although compositional and structural changes oppose each other, as fluorination enhances surface conductivity while annealing reduces it, structural changes have a significant impact on dielectric performance. Therefore, these contrasting events clearly destroyed the shallow surface traps and created deeper charge traps.

3.4. Dielectric spectroscopy

This type of measurement was applied to investigate the electric dielectric performance of treated BOPP samples under electro-thermal stresses. During treatment, the tertiary hydrogen atoms, secondary, and eventually primary (i.e., (CH_n) groups) were gradually substituted as the fluorination time progressed. Notably, the significant growth of dipole polarization of (CF_n) groups has a critical role in the polarization process. Sample surface molecules undergo cross-linking during fluorination, restricting orientation polarization [22].

The loss factor (tan δ) is an important parameter to measure energy dissipation and, hence, the dielectric performance efficiency of polymer films. The tan δ of the aged samples displayed a varying increase in the frequency range from 0.01 to 1 MHz higher than that of the Pure sample (Fig. 9). Samples FA2,

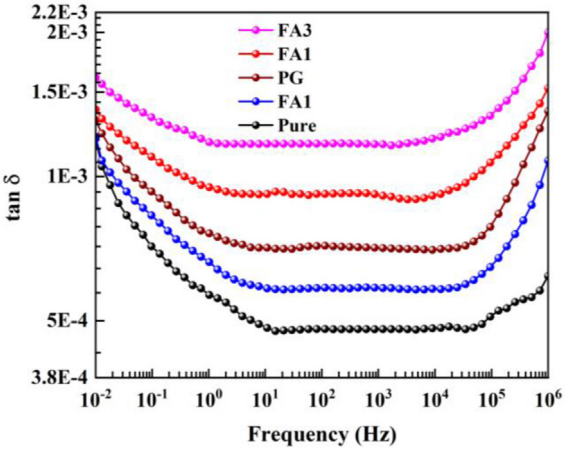

Fig. 9. The tan δ values for the pure and treated BOPP samples during application of the electro-thermal stresses.

PG, FA1, and FA3 all displayed varying increases in tan δ values by 0.8%, 9%, 15%, and 34%, respectively, at 0.01 Hz when compared to 4.8×10^{-4} for the Pure one. Meanwhile, they increased to 1.1×10^{-3}, 1.37×10^{-3}, 1.53×10^{-3}, and 2×10^{-3} due to an increase in dielectric relaxation loss as the frequency increased to 1 MHz.

Enhanced low-molecular-weight radicals involved in polarization often resulted in higher tan δ values. Therefore, the deposited fluorine layer on the surface of the FA1 failed to prevent space charges from being injected from the electrodes. This led to oxidation and degradation events and caused a noted increase in tan δ. In contrast, the fluorine deposited at 60 min introduced additional dipole moments and significantly increased the tan δ value of FA3. In this regard, changes in space charge dynamics and mechanisms caused by increased surface fluorine content can degrade dielectric properties. The local electric field is distorted as space charge accumulates within the dielectric, which increases the internal electromechanical stress and causes an increase in loss.

On the other hand, the fluorine layer at 30 min helped to prevent the accumulation of further space charges by increasing the surface conductivity. This resulted in a lesser increase in the tan δ value of the FA2 compared to the other samples. The dense fluorine layer also radically changed the depth of the charge trap and compensated for many of the surface defects responsible for creating space charge traps. The raised tan δ value of PG can be attributed to the impact of foreign materials and physical defects within the sample. These materials and defects activate as a catalytic mechanism to break the BOPP chains under the action of the electric field. Also, the tertiary protons in the film monomer units (CH_2CHCH_3) can make the film susceptible to oxidative degradation by free radical [34].

According to the mean value calculations of tan δ, samples FA2, PG, FA1, and FA3 have recorded an increase of 13%, 29%, 38.5%, and 87%, respectively, compared to the Pure one. These results revealed that the dielectric loss of FA2 did not show a significant increase and remained within the permitted limits. Consequently, this emphasizes the significance of surface treatments carried out with special care to enhance BOPP's aging resistance.

3.5. A.C. Conductivity

Under electro-thermal stresses, the dielectric properties are changed chemically and physically, increasing film conductivity. In this case, the dipole orientation and the migration of charge carriers brought on by space charge polarization could affect the mechanism of AC conductivity ($\sigma_{a.c.}$) [32]. A typical dielectric response indicates that $\sigma_{a.c}$ is independent at low frequencies, in accordance with the theory of dielectric physics. Yet, as shown in equation (2), the empirical power law shows that electrical conductivity increases at higher frequencies.

$$\boldsymbol{\sigma_{a.c}(\omega) = \omega\, \varepsilon_o \varepsilon''(\omega) = \sigma_{d.c} + A\, \omega^n} \quad (2)$$

The equation parameters indicate that ω is the angular frequency (radians per second), ε_o is the vacuum permittivity, and ε" is the loss factor of the dielectric or the imaginary part of the complex permittivity. While A is a material-specific temperature-dependent constant, n is a temperature- and frequency-dependent exponent in the range zero ≤ n ≤ unity, and $\sigma_{d.c}$ is the direct current conductivity. The aging process causes oxidation events and breaks the chains, hastening the decomposition of the film and enabling the release of more polar groups [33]. The development of the polar group within samples is evident by the apparent increase in $\sigma_{a.c.}$

Regardless, the σa.c curves show variations in the samples' conductivity depending on the circumstances of the surface treatments carried out, as depicted in Fig. 10. At frequencies higher than 0.1 Hz, the conductivity of samples PG, FA1, FA2, and FA3 increased according to the empirical power law. Compared with the Pure sample, the mean values for σa.c increased for the samples FA2, PG, FA1, and FA3 by 18.3%, 32.5%, 53.6%, and 67.7%, respectively. The σa.c values gradually increased and lost their frequency dependence, indicating that the PG, FA1, and FA3 samples degraded. The conductivity curves of the samples are represented as

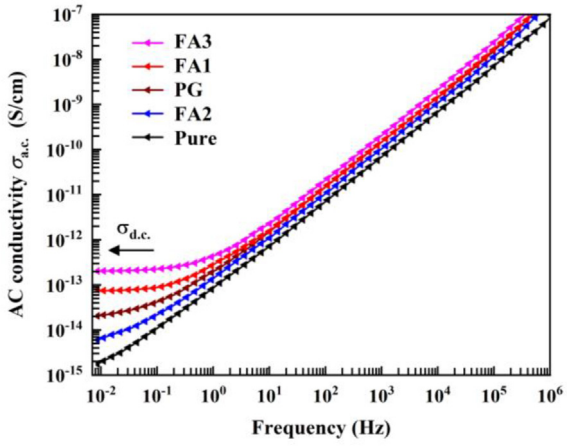

Fig. 10. AC conductivity patterns as a function of frequency at RT for pure and treated BOPP samples during electro-thermal stresses.

constant values at frequencies between 10^{-1} and 10^{-2}. The oxidation causes the formation of conjugated double-bond groups with the film's chemical structure. This will facilitate the electrons' mobility, impacting the overall conductivity [35].

As the electro-thermal stresses increased, the chemical composition of the polymer changed, causing new charge carriers to develop and enhancing their mobility within the film matrix. The noteworthy rise in σa.c of FA1 and FA3 at low frequencies is mostly due to the influence of interfacial polarization and the accumulation of charge carrier mobility [36].

3.6. Dynamic mechanical analysis

In this test, the FA3 sample was excluded due to its unsatisfactory results, which unequivocally showed a degradation in its properties. While the Pure, PG, and FA1 were tested as backgrounds for sample FA2. The storage modulus, loss modulus, and loss factor (tan delta) curves for samples are displayed in Fig. 11. The rise in crystallinity led to various increases in the storage and loss moduli. It should be noted that the storage modulus is greater in the crystalline region than in the amorphous one [37].

For the Pure, PG, AF1, and AF2 samples, the storage moduli generally started to decline at different temperatures at 3.32 °C, −7.17 °C, −9.98 °C, and −4.54 °C, respectively. In contrast, the storage moduli of samples Pure, PG, AF1, and AF2 began with values of about 2865, 3500, 1640, and 7000 Mpa, respectively. A higher storage modulus value indicates a greater ability of the material to store energy. Two temperature peaks can be seen in the loss modulus, which are roughly 1.76 °C and 32.25 °C for the Pure sample and roughly 1.53 °C and 136.07 °C for the PG sample, respectively. These peaks correspond to the β- and α-transitions for a film. In return, the loss modulus for the FA1 and FA2 samples revealed a single temperature peak at about 3.35 °C and 9.59 °C, respectively. The abrupt drop in loss modulus is associated with the material's relaxation time, the time required for chains to change in response to the applied stress. Thus, the

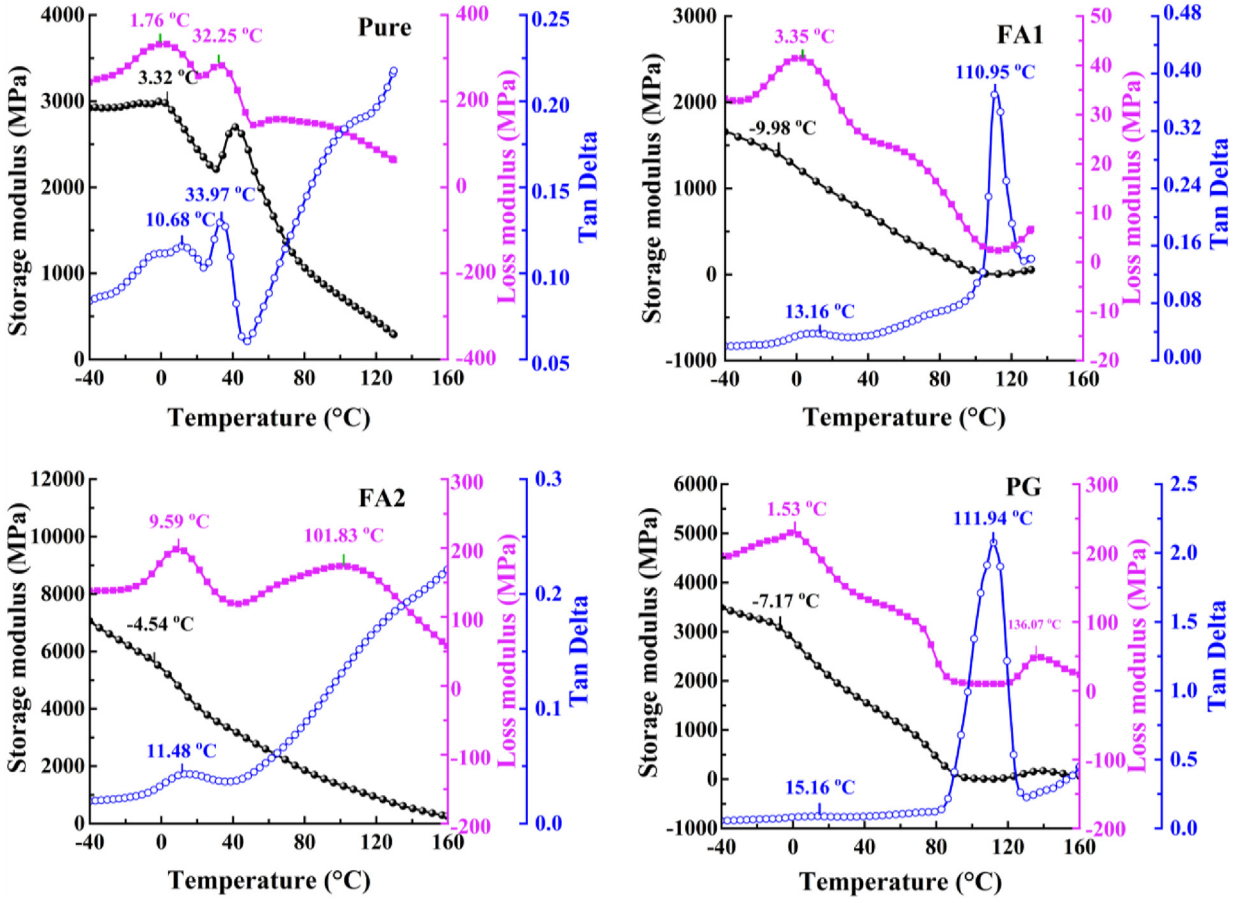

Fig. 11. DMA curves of storage modulus, loss modulus, and loss factor for the pure and treated BOPP samples during electro-thermal stresses.

material's viscous response is lost if it doesn't have enough time to flow.

The tan delta curve of the Pure sample revealed two peaks at 10.68 °C and 33.97 °C, which are attributed to the β- and α-transitions. In contrast to the Pure sample, the PG sample showed higher peaks at 15.16 °C and 111.94 °C, which indicated a definite shift toward a higher temperature. The tan delta curve showed peaks at 5.63 °C and 110.95 °C with regard to FA1, whereas it showed a single peak at 11.48 °C for sample FA2. The peak of the α-transition has moved to a higher temperature and, as a result, did not appear on the adopted temperature scale. Among many calculating methods that employ the loss modulus or the storage modulus, the glass transition temperature (T_g) was calculated using the tan delta curves. It represents the localized maximum of the loss factor on the curve. Tan delta curves offer data on the material's energy dissipation and viscoelastic behavior impacted by the glass transition.

The T_g of materials can thus be determined and studied using tan delta curves. The material–glass transition region is related to the tan delta peak because, in deformation conditions, the viscous response to the elastic response proportion is higher. The behavior of the T_g varied depending on the chemistry of each sample. The apparent peak in the pure sample at 10.68 °C is attributed to T_g, or β-relaxation. It was found that the PG sample has a T_g of 4.48 °C higher than that in the Pure. Meanwhile, it was observed that the T_g for the samples AF1 and AF2 increased by 2.48 °C and 0.92 °C, respectively, compared to the Pure one. The high T_g value of the PG sample indicates that chain cross-linking occurred as a result of the polymer chains' restriction on rotational motion.

The PG and AF1 samples' decreased loss modulus values indicate that the material changed from an elastic flow to a plastic flow behavior. The formation probability of micro- and nanovoids on the sample surface increased due to the significant degradation of ductility. The FA1 sample's comparatively low storage modulus was also attributed to cross-links or weak noncovalent chemicals that formed within the sample. The AF2 sample, on the other hand, retained its ductility and saw the least change in T_g value among samples, which enhanced its resistance to mechanical deformation [38].

The results imply improved thermal stability and resistance to deformation of the FA2 sample under raised temperatures. An acceptable slight increase in stiffness and a decrease in energy dissipation (i.e., the ability to dissipate energy while deforming) are indicators of the desired improvement.

4. Conclusion

The study methodology and result analysis have demonstrated the impacts of optimal fluorination and annealing processes on the properties of BOPP film. On the other hand, the treated samples' aging resistance behavior under electro-thermal stressors is investigated.

The following is a summary of the key conclusions:

1. The conflicting fluorination and annealing events on the FA2 surface resulted in enhanced crystallinity, surface roughness, and denser surface molecules. As a result, many physical interfaces to the charge traps and deep charge traps were established, accelerating the surface potential decay by 87.6%.
2. Charge traps formed mitigated the impacts of the electric field at the metal–dielectric interface and limited the injection of more charges into the FA2 sample. Thus, tan δ showed a slight increase of 13% and a limited conductivity increase of 18.3% for the FA2 sample, in contrast to the other samples that revealed a deterioration in their properties.
3. The AF2 sample showed improved mechanical properties manifested by a high storage modulus of 7000 MPa, a loss modulus temperature peak of 9.59 °C, and a T_g value evolution of 0.92 °C. These results indicate the sample's ability to resist gradual deformation, the highest energy dissipation, and favorable ductility under stress.

The results verified the effectiveness of surface treatments in enhancing BOPP film's aging resistance for capacitors. Yet, for an in-depth evaluation, more investigations are needed to determine the impact of surface treatments on other electrical properties of dielectric.

Acknowledgements

This work would not have been attainable without the support of the State Key Laboratory of Power Transmission Equipment and System Security and New Technology, School of Electrical Engineering, Chongqing University, and the Electrical and Electronic Engineering Department, University of Kerbala.

References

[1] H.M. Umran, F. Wang, Y. He, Ageing: causes and effects on the reliability of polypropylene film used for HVDC capacitor, J IEEE Access 8 (2020) 40413–40430, https://doi.org/10.1109/ACCESS.2020.2976526.

[2] H.F. Alesary, H.K. Ismail, A.H. Odda, M.J. Watkins, A.A. Majhool, A.D. Ballantyne, K.S. Ryder, Influence of different concentrations of nicotinic acid on the electrochemical fabrication of copper film from an ionic liquid based on the complexation of choline chloride-ethylene glycol, J Electroanal Chem 897 (2021) 115581, https://doi.org/10.1016/j.jelechem.2021.115581.
[3] V.O. Belko, O.A. Emelyanov, I.O. Ivanov, D.Y. Glivenko, Metallized film capacitors degradation under high electrodynamic load, in: 2017 IEEE Conf. of Ru. Young Researchers in Elec. and Electron. Eng. (EIConRus), St. Petersburg and Moscow, Russia, 2017, pp. 1120–1122, https://doi.org/10.1109/EIConRus.2017.7910753.
[4] S.A. Ashter, 3-Review of characteristics of common plastics for thermoforming, in: S.A. Ashter, eds., Thermoforming of Single and Multilayer Laminates, William Andrew Publishing, Oxford. 2014, pp. 39–63, https://doi.org/10.1016/B978-1-4557-3172-5.00003-7.
[5] A. Kahouli, O. Gallot-Lavallée, P. Rain, O. Lesaint, L. Heux, C. Guillermin, J.M. Lupin, Structure effect of thin film polypropylene view by dielectric spectroscopy and X-ray diffraction: application to dry type power capacitors, J Appl Polym Sci 132 (1 of 7) (2015) 42602, https://doi.org/10.1002/app.42602.
[6] H.M. Umran, F. Wang, Y. He, Improved electrical performance of BOPP films by acidic treatment at an elevated temperature, in: 2020 Int. Conf. on Diagnostics in Electr. Eng. (Diagnostika), IEEE., Pilsen, Czech Republic, 2020, pp. 1–4, https://doi.org/10.1109/Diagnostika49114.2020.9214759.
[7] F. Zheng, C. Lin, C. Liu, Z. An, Q. Lei, Y. Zhang, A method to observe fast dynamic space charge in thin dielectric films, J Appl Phys Lett 101 (2012) 172904, https://doi.org/10.1063/1.4763473.
[8] V.O. Belko, O.A. Emelyanov, I.O. Ivanov, A.P. Plotnikov, Self-healing processes of metallized film capacitors in overload modes—Part 1: experimental observations, J IEEE Trans Plasma Sci 49 (2021) 1580–1587, https://doi.org/10.1109/TPS.2021.3071187.
[9] G. Zhang, C. Nam, L. Petersson, J. Jämbeck, H. Hillborg, T.M. Chung, Increasing polypropylene high temperature stability by blending polypropylene-bonded hindered phenol antioxidant, J Macromol 51 (2018) 1927–1936, https://doi.org/10.1021/acs.macromol.7b02720.
[10] M.Z. Saleem, M. Akbar, Review of the performance of high-voltage composite insulators, J Polym (Basel) 14 (2022) 431, https://doi.org/10.3390/polym14030431.
[11] M.J.J. Fernandez, K. Abirami, S. Swetha, S. Soundarya, N. Rasana, K. Jayanarayanan, The effect of nano, micro and dual scale filler reinforcement on the morphology, mechanical and barrier properties of polypropylene composites, J Mater Today: SAVE Proc 46 (2021) 5067–5071, https://doi.org/10.1016/j.matpr.2020.10.424.
[12] Z. Xie, D. Liu, K. Wu, Q. Fu, Improved dielectric and energy storage properties of polypropylene by adding hybrid fillers and high-speed extrusion, J Polytech 214 (1–9) (2021) 123348, https://doi.org/10.1016/j.polymer.2020.123348.
[13] B.X. Du, Z.L. Li, J. Li, Surface charge accumulation and decay of direct-fluorinated RTV silicone rubber, J IEEE Trans Dielectr Electr Insul 21 (2014) 2338–2342, https://doi.org/10.1109/TDEI.2014.004079.
[14] X. Wang, Z. An, M. Zhuo, Energy storage performance and dielectric properties of surface fluorinated BOPP films, J IEEE Trans Dielectr Electr Insul 30 (2023) 1950–1957, https://doi.org/10.1109/TDEI.2023.3280862.
[15] Z. Lv, H. Li, J. Song, Z. Chen, W. Jia, F. Guo, K. Wu, Y. Cheng, Study on the influential mechanism of fluorination on the flashover voltage of polypropylene film under nanosecond pulse voltage, J IEEE Trans Dielectr Electr Insul 29 (2022) 1433–1440, https://doi.org/10.1109/TDEI.2022.3179993.
[16] N.A. Belov, A.Y. Alentiev, Y.G. Bogdanova, A.Y. Vdovichenko, D.S. Pashkevich, Direct fluorination as method of improvement of operational properties of polymeric materials, J Polym 12 (1–24) (2020) 2836, https://doi.org/10.3390/polym12122836.
[17] M. Namie, J.H. Kim, S. Yonezawa, Enhanced dyeing of polypropylene using fluorine–oxygen gas mixtures, J Colorants 2 (2023) 552–564, https://doi.org/10.1063/1.5088335.
[18] H. Bayazian, A. Yadgari, J. Morshedian, A. Jamshidi, M. Razavi-Nouri, Evaluation of morphology and crystallinity of biaxially oriented polypropylene films, J AIP Conf Proc 2065 (2019) 1–4, https://doi.org/10.1063/1.5088335.
[19] X. Dai, Z. Xing, W. Yang, C. Zhang, F. Li, X. Chen, C. Li, J. Zhou, L. Li, The effect of annealing on the structure and electric performance of polypropylene films, Int J Polym Sci 2022 (2022) 1–12, https://doi.org/10.1155/2022/5970484.
[20] Z. An, J. Yao, M. Mao, Y. Zhang, Z. Xia, Significantly improved charge stability of cellular polypropylene films by fluorination and subsequent annealing, J Electrost 68 (2010) 523–527, https://doi.org/10.1016/j.elstat.2010.07.003.
[21] Y. Ren, H. Zou, S. Wang, J. Liu, D. Gao, C. Wu, S. Zhang, Effect of annealing on microstructure and tensile properties of polypropylene cast film, Colloid Polym Sci 296 (2018) 41–51, https://doi.org/10.1007/s00396-017-4220-8.
[22] X. Wu, X. Chen, Q.M. Zhang, D.Q. Tan, Advanced dielectric polymers for energy storage, Energy Storage Mater 44 (2022) 29–47, https://doi.org/10.1016/j.ensm.2021.10.010.
[23] D. Min, M. Cho, A.R. Khan, S. Li, Charge transport properties of dielectrics revealed by isothermal surface potential decay, J IEEE Trans Dielectr Electr Insul 19 (2012) 1465–1473, https://doi.org/10.1109/TDEI.2012.6260024.
[24] B.X. Du, J. Li, W. Du, Dynamic behavior of surface charge on direct-fluorinated polyimide films, J IEEE Trans Dielectr Electr Insul 20 (2013) 947–954, https://doi.org/10.1109/TDEI.2013.6518964.
[25] G.M. Sessler, M.T.D. Figueiredo, G.L. Ferreira, Models of charge transport in electron-beam irradiated insulators, J IEEE Trans Dielectr Electr Insul 11 (2004) 192–202, https://doi.org/10.1109/TDEI.2004.1285887.
[26] A. Rjeb, L. Tajounte, M. Chafik El Idrissi, S. Letarte, A. Adnot, D. Roy, Y. Claire, A. Périchaud, J. Kaloustian, IR spectroscopy study of polypropylene natural aging, J Appl Polym Sci 77 (2000) 1742–1748, https://doi.org/10.1002/1097-4628(20000822)77:8<1742::AID-APP11>3.0.CO;2-T.
[27] X. Li, J. Pan, F. Macedonio, C. Ursino, M. Carraro, M. Bonchio, E. Drioli, A. Figoli, Z. Wang, Z. Cui, Fluoropolymer membranes for membrane distillation and membrane crystallization, J Polym 14 (2022) 5439, https://doi.org/10.3390/polym14245439.
[28] B. Sharmila, N. George, S. Sasi, J. V Antony, J. Chandra, V. Raman, D. Nambath Purushothaman, A comprehensive investigation of dielectric properties of epoxy composites containing conducting fillers: fluffy carbon black and various types of reduced graphene oxide, J Polym Adv Technol 33 (2022) 3151–3162, https://doi.org/10.1002/pat.5767.
[29] C. Angelloz, R. Fulchiron, A. Douillard, B. Chabert, R. Fillit, A. Vautrin, L. David, Crystallization of isotactic polypropylene under high pressure (γ phase), J Macromol 33 (2000) 4138–4145, https://doi.org/10.1021/ma991813e.
[30] R.H. Somani, B.S. Hsiao, A. Nogales, H. Fruitwala, S. Srinivas, A.H. Tsou, Structure development during shear flow induced crystallization of i-PP: in situ wide-angle X-ray diffraction study, J Macromol 34 (2001) 5902–5909, https://doi.org/10.1021/ma0106191.
[31] E. Lezak, Z. Bartczak, Plastic deformation of the γ phase isotactic polypropylene in plane– strain compression at elevated temperatures, J Macromol 40 (2007) 4933–4941, https://doi.org/10.1021/ma0708038.
[32] B. Sharmila, N. George, S. Sasi, V. Antony, J. Chandra, V. Raman, D. Nambath Purushothaman, A comprehensive investigation of dielectric properties of epoxy composites containing conducting fillers: fluffy carbon black and various types of reduced graphene oxide, J Polym Adv Technol 33 (2022) 3151–3162, https://doi.org/10.1002/pat.5767.

[33] I. Liguori, G. Russo, F. Curcio, G. Bulli, L. Aran, D. Della-Morte, G. Gargiulo, G. Testa, F. Cacciatore, D. Bonaduce, P. Abete, Oxidative stress, aging, and diseases, J Clin Interv Aging 13 (2018) 757–772, https://doi.org/10.2147/CIA.S158513.
[34] M. Murzakanova, T. Borukaev, M. Begretov, A. Mikitaev, The degradation of polyethylene and mechanisms of its stabilisation by azomethinephenylmelamine compounds, J Int Polym Sci Technol 41 (2014) 43–48, https://doi.org/10.1177/0307174X1404101110.
[35] S. Fratini, M. Nikolka, A. Salleo, G. Schweicher, H. Sirringhaus, Charge transport in high-mobility conjugated polymers and molecular semiconductors, J Nat Mater 19 (2020) 491–502, https://doi.org/10.1038/s41563-020-0647-2.
[36] M. Samet, A. Kallel, A. Serghei, Maxwell-Wagner-Sillars interfacial polarization in dielectric spectra of composite materials: scaling laws and applications, J Compos Mater 56 (2022) 3197–3217, https://doi.org/10.1177/00219983221090629.
[37] L. Cheng, W. Liu, X. Liu, C. Liu, S. Li, Z. Xing, Online degradation of biaxial-orientated polypropylene film from HVDC filter capacitors, J IEEE Trans Dielectr Electr Insul 26 (2019) 26–33, https://doi.org/10.1109/TDEI.2018.007386.
[38] X. Yuan, T.C. Chung, Cross-linking effect on dielectric properties of polypropylene thin films and applications in electric energy storage, J Appl Phys Lett 98 (2011) 062901, https://doi.org/10.1063/1.3552710.